ACS APPLIED MATERIALS & INTERFACES

Research Article

www.acsami.org

Two-Photon Induced Photoluminescence and Singlet Oxygen Generation from Aggregated Gold Nanoparticles

Cuifeng Jiang,[†] Tingting Zhao,[†] Peiyan Yuan,[†] Nengyue Gao,[†] Yanlin Pan,[†] Zhenping Guan,[†] Na Zhou,[†] and Qing-Hua Xu*[,†,‡]

[†]Department of Chemistry, National University of Singapore, 3 Science Drive 3, Singapore 117543

[‡]National University of Singapore (Suzhou) Research Institute (NUSRI), Suzhou, Jiangsu, China 215123

ABSTRACT: Metal nanoparticles have potential applications as bioimaging and photosensitizing agents. Aggregation effects are generally believed to be adverse to their biomedical applications. Here we have studied the aggregation effects on two-photon induced photoluminescence and singlet oxygen generation of Au nanospheres and Au nanorods of two different aspect ratios. Aggregated Au nanospheres and short Au nanorods were found to display enhanced two-photon induced photoluminescence and singlet oxygen generation capabilities compared to the unaggregated ones. The two-photon photoluminescence of Au nanospheres and short Au nanorods were enhanced by up to 15.0- and 2.0-fold upon aggregation, and the corresponding two-photon induced singlet oxygen generation capabilities were enhanced by 8.3 and 1.8-fold, respectively. The two-photon induced photoluminescence and singlet oxygen generation of the aggregated long Au nanorods were found to be lower than the unaggregated ones. These results support that the change in their two-photon induced photoluminescence and singlet oxygen generation originate from aggregation modulated two-photon excitation efficiency. This finding is expected to foster more biomedical applications of metal nanoparticles as Au nanoparticles normally exist in an aggregated form in the biological environments. Considering their excellent biocompatibility, high inertness, ready conjugation, and easy preparation, Au nanoparticles are expected to find more applications in two-photon imaging and two-photon photodynamic therapy.

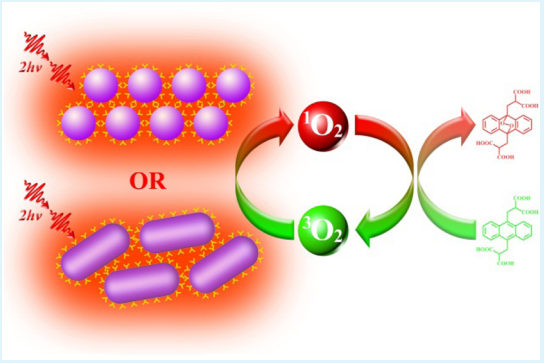

KEYWORDS: *gold nanoparticles, plasmon coupling, two-photon excitation, singlet oxygen generation, two-photon photoluminescence*

INTRODUCTION

Noble metal nanoparticles, such as Au and Ag, display many unique optical properties including localized surface plasmon resonance (LSPR), which arises from collective oscillation of the conduction band electrons.[1−4] The LSPR frequency is sensitive to the particle size, shape, dielectric properties of their surrounding media and the coupling between the nanoparticles.[5−8] Plasmon resonance of metal nanoparticles has been utilized to modulate the optical properties of nearby chromphores or themselves, such as surface-enhanced Raman scattering[9−11] and plasmon enhanced fluorescence.[12−16] Metal nanoparticles are generally known to be "non-fluorescent" under conventional one-photon excitation because of their low emission quantum yields.[17,18] Gold nanorods (Au NRs) have been demonstrated to display strong two-photon photoluminescence (TPPL) with brightness 58 times stronger than the conventional organic chromophores.[19] Au NRs have thus been utilized in two-photon imaging and photothermal cancer therapy.[20−25] Spherical metal nanoparticles, such as Au, Ag, and Pt, were recently demonstrated to sensitize the formation of singlet oxygen directly and could potentially act as excellent photosensitizers for photodynamic therapy because of their superior photostability and resistance to enzymatic degradation.[26] Our recent work demonstrated that Au NRs of different aspect ratios could act as excellent nanophotosensitizers to sensitize the formation of singlet oxygen under two-photon excitation.[25]

Many previous studies showed that aggregation of metal nanoparticles can be induced by small molecules or ionic species.[6,27−40] Metal nanoparticles easily aggregate in the biological environment. Aggregation of nanoparticles were generally believed to be disadvantageous or a potential problem for their biomedical applications.[41−43] Our recent work, however, demonstrated that aggregation of Au and Ag nanospheres and Au nanocubes resulted in significantly enhanced TPPL by up to 100-fold in solution and 5 orders of magnitude on the single particle level due to plasmon coupling.[44−47] The enhancement was ascribed to enhanced two-photon excitation because of formation of a longitudinal Plasmon mode and enhanced local field at the excitation wavelength.[48,49] Plasmon coupling enhanced TPPL of Ag and Au NPs have been further utilized to develop two-photon sensing platforms for detection of mercury,[50] cysteine, and glutathione.[46] Metal nanoparticles have been recently demon-

Received: February 27, 2013
Accepted: May 20, 2013
Published: May 20, 2013

strated to sensitize the formation of singlet oxygen directly under one- and two-photon excitation and could potentially act as photosensitizers for photodynamic therapy.[25,26] It is important to understand the aggregation effects on two-photon induced singlet oxygen generation capability of various metal nanoparticles and their applications as two-photon photosensitizers. Herein we report the aggregation effects on TPPL and two-photon induced singlet oxygen generation for Au nanospheres (NSs) and Au nanorods (NRs) of two different aspect ratios. Our results demonstrated that both enhancement and quenching in TPPL and two-photon induced singlet oxygen generation could be resulted, depending on the shape and aspect ratios of the metal nanoparticles. These studies provide insight on choice of metal nanoparticles in their applications in two-photon imaging, sensing and phototherapy.

EXPERIMENTAL SECTION

Materials. Trisodium citrate was purchased from BDH Chemical Ltd. Cetyltrimethylammonium bromide (CTAB) and ascorbic acid were purchased from Alfa Aesar. Cysteine, silver nitrate ($AgNO_3$), sodium borohydride ($NaBH_4$), hydrogen tetrachloroaurate (III) hydrate ($HAuCl_4 \cdot 3H_2O$), and 9,10-anthracenediyl-bis(methylene) dimalonic acid (ABDA) were purchased from Sigma Aldrich. All solvents are of analytical grade and used as received without further purification. All aqueous solutions are prepared in deionized water.

Preparation and Assembly of Gold Nanoparticles. Gold nanospheres (Au NSs) were prepared by citrate reduction of chloroauric acid.[51] Briefly, 50 mL of $HAuCl_4$ solution (10^{-2} % by weight) was heated to boiling and 0.4 mL of trisodium citrate solution (1% by weight) was subsequently added. The solution turned faintly blue (nucleation) after 25 s and changed into a brilliant red after 1 min. The solution was allowed to react for another 30 min under stirring to form the final Au nanoparticles. The assembly process of gold nanospheres was triggered by addition of different amounts of 0.1 M cysteine.[52]

Gold nanorods (Au NRs) were prepared according to a previously reported method.[53−55] Briefly, CTAB aqueous solution (0.1 M, 10 mL) was mixed with $HAuCl_4$ (50 mM, 50 μL) and ice-cold $NaBH_4$ (10 mM, 0.6 mL) to form a brownish-yellow seed solution. This seed solution was kept at room temperature for at least 2 h. In the growth solution, CTAB solution (0.1 M, 10 mL) was mixed with $HAuCl_4$ (50 mM, 0.1 mL), different amount of $AgNO_3$ (10 mM, 63 or 81 μL), HCl (1.0 M, 0.2 mL), and ascorbic acid (0.1 M, 80 μL). The color of the growth solution changed to colorless upon gentle mixing. The gold seed solution (25 μL) was then added into the growth solution and the reaction mixture was left undisturbed overnight. The obtained Au NRs were purified by washing with deionized water to remove excess CTAB and redispersed in deionized water. The assembly process of Au NRs is triggered by adding different amounts of 0.1 M cysteine after adjusting the pH of the solution to 3.5 using HCl.[56]

Detection of Singlet Oxygen Generation. Singlet oxygen generation under two-photon excitation was monitored by chemical oxidation of ABDA in water solution. ABDA can react irreversibly with singlet oxygen, leading to a decrease in the ABDA absorption at 380 nm. The sample solution was prepared by mixing isolated (unaggregated) or aggregated Au nanoparticles with ABDA. The solutions were irradiated by an unfocused femtosecond laser beam (beam area = 0.3 cm^2) at 800 nm with pulse duration of 60 fs and repetition rate of 1 kHz and energy power density of 3.0 Wcm^{-2}, which are generated from an amplifier laser system (Spectra Physics Spitfire Pro). The absorbance of the solution at 380 nm was recorded at 2 min intervals by measuring their UV−vis spectra.

Instrumentations and Characterizations. Transmission electron microscopic (TEM) images of the nanoparticles were recorded by using a JEOL 2010 microscope. Ultraviolet−visible (UV−vis) extinction spectra were measured by using a Shimadzu UV-2550 spectrophotometer. Two-photon excitation photoluminescence measurements were performed by using an Avesta TiF-100 M Ti:sapphire oscillator as the excitation source, which gives output laser pulses with central wavelength at 800 nm, pulse duration of 80 fs and a repetition rate of 84.5 MHz. The laser beam was focused onto the samples that were contained in a cuvette. The emission from the samples was collected at a 90° angle by a pair of lenses and an optical fiber that was connected to a monochromator (Acton, Spectra Pro 2300i) coupled CCD (Princeton Instruments, Pixis 100B) system. A short pass filter with a cutoff wavelength of 750 nm was placed before the spectrometer to minimize the scattering from the excitation beam.

RESULTS AND DISCUSSION

Au NSs and Au NRs of two different aspect ratios (representative for short and long Au NRs) were prepared to investigate the aggregation effects on their TPPL and two-photon induced singlet oxygen generation capability. Au NSs were prepared by using a citrate reduction method.[51] Au NRs were prepared by using a seed-mediated, CTAB-assisted method with aspect ratios controlled by the amount of $AgNO_3$. The representative TEM images of the obtained Au NSs and Au NRs are shown in Figurea 1a, 1c, and 1e. The

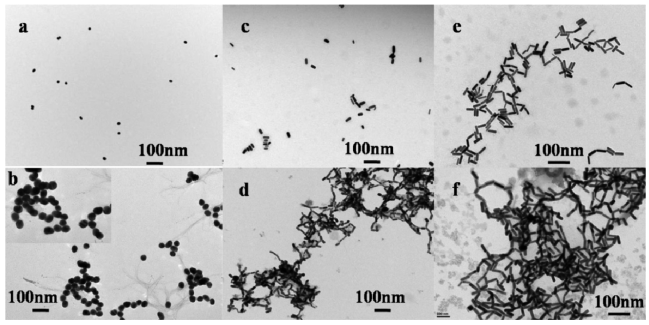

Figure 1. TEM images of (a, c, e) isolated and (b, d, f) aggregated (a, b) Au NSs, (c, d) short Au NRs, and (e, f) long Au NRs.

obtained Au NSs are uniform with a diameter of 40 nm (Figure 1a) with LSPR band centered at 529 nm. The short and long Au NRs have aspect ratios of 2.3 and 3.5, with longitudinal LSPR band maximum at 650 and 780 nm respectively, consistent with the Gan's theory.[57]

Coupling of Au nanoparticles were induced by addition of cysteine. Cysteine is an amino acid containing a thiol-group that can bind to the surface of Au nanoparticles. In the acidic environment, cysteine forms a zwitterionic structure and the cooperative two-point electrostatic interactions induce the coupling of Au nanoparticles.[56,58] Upon the addition of cysteine, Au NSs solution rapidly changed the color from red to purple, indicating the formation of Au nanoparticle aggregates. The aggregate formation was confirmed by both their TEM images (Figure 1b) and extinction spectra (Figure 2a). The addition of cysteine resulted in a decrease in the original LSPR band at 529 nm companied by appearance of a new band in the longer wavelength region. This new LSPR band corresponds to the longitudinal mode along the long axis of coupled nanostructures and gradually shifted to longer wavelengths with increasing cysteine concentration. For both short and long Au NRs, the original longitudinal peak at 650 and 780 nm decreased upon the gradual addition of cysteine, accompanied by appearance of new SPR band at the longer wavelength region (Figure 2b,c). Both the extinction spectra change and TEM images confirm the formation of Au nanoparticle aggregates.

dx.doi.org/10.1021/am4007403 | ACS Appl. Mater. Interfaces 2013, 5, 4972−4977

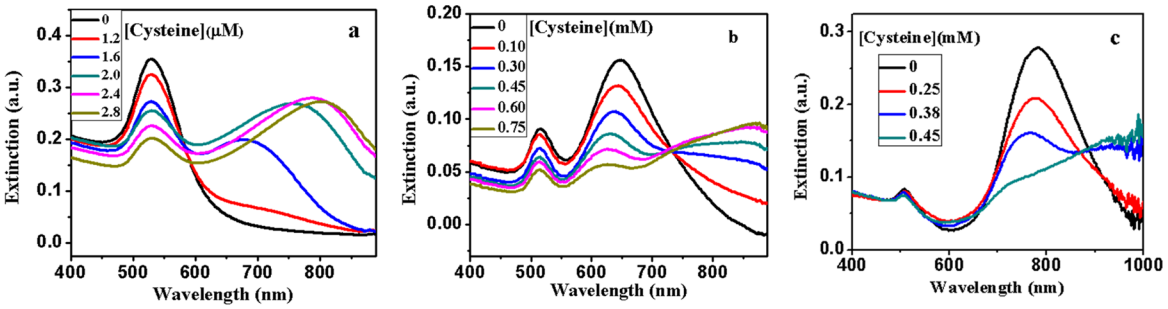

Figure 2. Extinction spectra of (a) Au NSs, (b) short Au NRs, and (c) long Au NRs before and after addition of different amounts of cysteine.

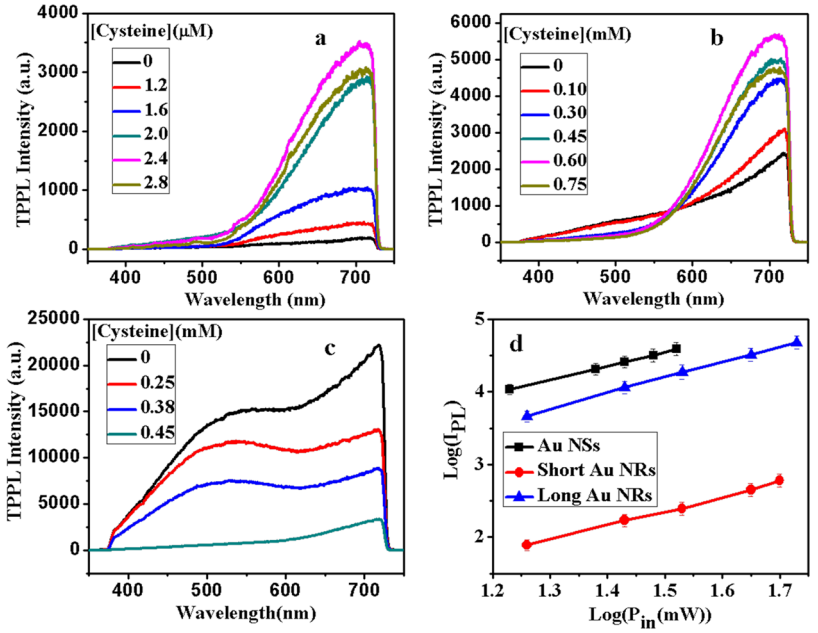

Figure 3. TPPL spectra of (a) Au NSs, (b) short Au NRs, and (c) long Au NRs under excitation at 800 nm using femtosecond laser pulses (excitation power: 50 mW); (d) excitation power dependence of TPPL for aggregated Au NSs, short and long Au NRs. Error bars represent standard deviations for measurements taken from three independent experiments.

Two-photon photoluminescence (TPPL) spectra of isolated (unaggregated) and aggregated Au NSs and two types of Au NRs (Figure 3) were measured by using femtosecond laser pulses at 800 nm as the excitation source. The TPPL spectra were rather broad for both Au NSs and Au NRs. The TPPL intensity of the coupled Au NSs gradually increased upon addition of cysteine to induce the aggregation and an optimum enhancement factor of 15.0 fold was observed when cysteine concentration of 2.4 μM was added. The TPPL spectra of Au NRs of two different aspect ratios displayed very different behaviors upon aggregation. Upon gradual addition of cysteine, the emission of the short Au NRs in the shorter wavelength range (<570 nm) decreased, whereas the longer wavelength portion (>570 nm) increased first and then decreased. The maximum enhancement factor of 2.2-fold in the integrated emission in the visible range was achieved when [cysteine] was 0.60 mM. For long Au NRs, the TPPL intensity in the detected visible range steadily decreased with gradual addition of cysteine. When [cysteine] reached 0.45 mM, the emission band in the visible range disappeared and only a tail was observed, consistent with the disappearance of longitudinal SPR peak at 780 nm in their extinction spectra (Figure 2c). Further addition of cysteine will cause precipitation of long Au NRs.

The two-photon excitation nature of the observed emission was confirmed by measuring the integrated emission intensity as a function of the laser excitation power density (Figure 3d). The best-fitting straight line of log−log plot gave a slope of 1.9, 2.0, and 2.15 for Au NSs, short and long Au NRs, respectively, confirming the involvement of two photons in the excitation process of the observed emission. The enhanced TPPL observed in aggregated Au NSs and short Au NRs could be explained as a result of increased extinction at the excitation wavelength, as plasmon coupling in the aggregated metal NPs results in the formation of a longitudinal band that is strongly resonant with the excitation wavelength. This new longitudinal band provides intermediate states that greatly promote two-photon excitation processes.[45,49,50] On the other hand, the enhanced local electric field near the excitation wavelength due to plasmon coupling also contributes to the enhanced TPPL.[59] The quenched TPPL of long Au NRs upon aggregation could be explained by a similar fashion. Upon the formation of the aggregate of long Au NRs, the extinction at the excitation wavelength (800 nm) decreases (Figure 2c), which results in a decreased intermediate absorption and reduced local electric field at 800 nm, consequently reduced two-photon excitation efficiency and quenched TPPL intensities.

dx.doi.org/10.1021/am4007403 | ACS Appl. Mater. Interfaces 2013, 5, 4972−4977

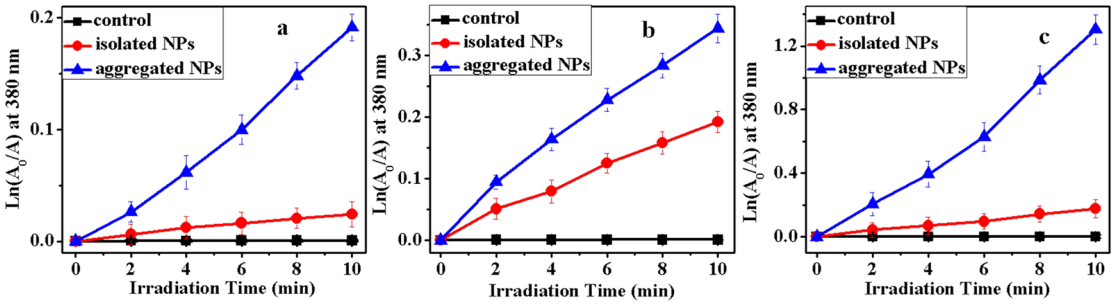

Figure 4. Photo-oxidation of ABDA as a function of irradiation time in the presence of isolated (unaggregated) and aggregated (a) Au NSs, (b) short Au NRs, and (c) long NRs. A_0 and A are the absorbance of ABDA at 380 nm before and after laser irradiation, respectively. Error bars represent standard deviations for measurements taken from three independent experiments.

Efficient singlet oxygen ($^1O_2$) generation is a prerequisite for application of photosensitizers in photodynamic therapy.[60] Since both two-photon induced $^1O_2$ generation and TPPL originate from two-photon excitation, plasmon coupling is expected to modulate the two-photon induced $^1O_2$ generation in a similar fashion. Singlet oxygen generation capability of aggregated Au NPs under two-photon excitation was evaluated by a chemical method using 9,10-anthracenediyl-bis-(methylene) dimalonic acid (ABDA). ABDA converts to its endoperoxide in the presence of $^1O_2$, leading to a decrease in ABDA absorption. The aggregated Au nanoparticle samples with maximum TPPL modulation, Au NSs with 0.24 μM of cysteine, short Au NRs with 0.60 mM of cysteine, and long Au NRs with 0.48 mM of cysteine were chosen for the experiments. Under these conditions, optimum TPPL enhancement was observed for Au NSs and short NRs while largest TPPL quenching effect was observed for stable long Au NRs aggregates. Direct photo-oxidation of ABDA samples without any Au nanoparticles under laser irradiation was also performed under the same experimental condition as the control. The decreasing ABDA absorbance at 380 nm as a function of irradiation time in the presence of various Au nanoparticles under illumination of femtosecond laser pulses at 800 nm was shown in Figure 4. It can be seen that the absorbance at 380 nm steadily decreased in the presence of both isolated (unaggregated) and aggregated Au nanoparticles. However, photo-oxidation rate of ABDA in the presence of various Au nanoparticles changed significantly when aggregated Au nanoparticles were used. The photo-oxidation rate constants (k_{obs}) of ABDA were obtained by assuming first-order kinetics and the results are summarized in Table 1. The photo-oxidation rates of ABDA in the presence of aggregated Au NSs and short Au NRs are 8.3 and 1.8 times of those of unaggregated ones. The photo-oxidation rate of ABDA in the presence of aggregated long Au NRs is slower compared to the unaggregated ones (enhancement factor of 0.13-fold). The photo-oxidation rate is an indicator of singlet oxygen generation capability of Au nanoparticles under two-photon excitation. These results suggest that the singlet oxygen generation capability of aggregated Au NSs, short Au NRs and long Au NRs are 8.3, 1.8, and 0.13 times those of unaggregated ones. The overall trend is consistent with their TPPL intensity changes upon aggregation (15.0, 2.2, and 0.08-folds for Au NSs, short Au NRs, and long Au NRs, respectively, see Figure 5). These results further confirm that change in

Table 1. Optical Properties of Au Nanoparticles

samples	k_{obs} ($\times 10^{-2}$ s^{-1})[a]	two-photon action cross-section ($\phi\delta$, GM/particle)[b]
isolated Au NSs (λ_{max} = 529 nm)	0.24	4×10^2
aggregated Au NSs	2.0	5×10^3
isolated short Au NRs (λ_{max} = 650 nm)	1.9	2.2×10^3
aggregated short Au NRs	3.4	6.8×10^3
isolated long Au NRs (λ_{max} = 780 nm)	13	2.5×10^4
aggregated long Au NRs	1.7	5.2×10^3

[a]ABDA photo-oxidation rate constant. [b]Two-photon action cross section at 800 nm. The measurements were conducted in water solution using the Au NRs with aspect ratio of 4 as standard.

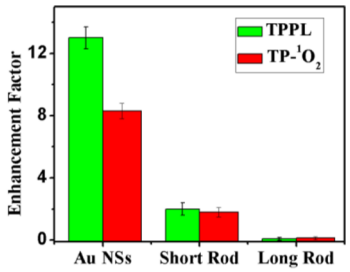

Figure 5. Enhancement factor of two-photon photoluminescence (TPPL) and two-photon induced $^1O_2$ generation (TP–$^1O_2$) for Au NSs, short Au NRs, and long Au NRs upon aggregation. Error bars represent standard deviations for measurements taken from three independent experiments.

TPPL intensities of aggregated Au nanoparticles are primarily due to change in their two-photon excitation efficiency, which in turn modulate the two-photon induced singlet oxygen generation capability correspondingly.

To gain more insight on the enhancement mechanism of singlet oxygen generation from aggregated Au NPs, TPPL properties and two-photon induced singlet oxygen generation capabilities of isolated and aggregated Au nanoparticles are summarized in Table 1 and Figure 5. Two-photon action cross section ($\phi\delta$, where δ is the two-photon absorption cross section and ϕ is the emission quantum efficiency) of unaggregated and aggregated Au nanoparticles were calculated by using Au NRs with an aspect ratio of 4 as the reference ($\phi\delta$ of 3×10^4 GM).[61] Two-photon action cross section is a direct indicator of the two-photon imaging capability. The enhancement factors of TPPL and two-photon induced singlet oxygen generation capability (TP–$^1O_2$) in Figure 5 were defined as the ratios of integrated TPPL intensity (or $\phi\delta$) and ABDA photo-oxidation rate constant for aggregated NPs to those for the corresponding

dx.doi.org/10.1021/am4007403 | ACS Appl. Mater. Interfaces 2013, 5, 4972–4977

isolated NPs before addition of any cysteine (the data in Table 1). The change in two-photon induced singlet oxygen generation upon aggregation was found to be consistent with the aggregation induced change in their TPPL, which is expected since both arise from two-photon excitation processes. The two-photon excitation efficiency was modulated significantly upon formation of aggregates.[49]

Noble metal nanospheres were previously demonstrated to sensitize the formation of singlet oxygen generation.[26] We have previously demonstrated that Au NRs displayed high two-photon-induced singlet oxygen generation capability (characterized by product of δ and singlet oxygen generation efficiency),[25] in addition to their large two-photon action cross-sections.[61,62] Au nanoparticles are promising in acting as contrast agents for biomedical applications such as cancer diagnosis, bioimaging, and cancer therapy, because of their excellent optical properties.[63] However, aggregation effects were generally assumed to be a potentially negative effect on their applications to reduce their efficiency. Our results show that two-photon action cross sections and two-photon induced singlet oxygen generation capability of Au NSs and short Au NRs increase upon the aggregation, although those of long Au NRs decrease after aggregation. Although aggregation effect will give a negative influence on application of long Au NRs in two-photon imaging and photosensitization, it can become advantageous for applications of Au NSs and short Au NRs.

CONCLUSIONS

In summary, we have examined the aggregation effects on TPPL and two-photon induced singlet oxygen generation capability of Au NSs and Au NRs of two different aspect ratios. TPPL and two-photon induced singlet oxygen generation were found to display a similar trend upon aggregation. Aggregated Au NSs and short Au NRs were found to display enhanced TPPL and singlet oxygen generation capabilities compared to the unaggregated ones. The TPPL of Au NSs and short Au NRs were found to be enhanced by up to 15.0- and 2.0-fold upon aggregation, with corresponding improvement in two-photon-induced singlet oxygen generation by 8.3- and 1.8-fold, respectively. The TPPL and two-photon induced singlet oxygen generation of the aggregated long Au NRs were lower than the unaggregated ones. These results support that the change in their TPPL intensities and two-photo induced singlet oxygen generation originate from aggregation modulated two-photon excitation efficiency. This finding is expected to foster more biomedical applications of noble metal nanoparticles. Spherical Au nanoparticles were generally believed to be unfavorable for applications of two-photon imaging and two-photon photodynamic therapy due to relative small two-photon absorption cross section. However, their two-photon action cross-section and two-photon singlet oxygen generation capability could be significantly improved through coupling. Au nanoparticles normally exist in an aggregated state inside the cells. Considering their excellent biocompatibility, high inertness, ready conjugation, and easy preparation, Au nanoparticles are expected to find more applications in two-photon imaging and two-photon photodynamic therapy.

AUTHOR INFORMATION

Corresponding Author

*E-mail: chmxqh@nus.edu.sg.

Notes

The authors declare no competing financial interest.

ACKNOWLEDGMENTS

This work was supported by DSTA Singapore (Project DSTA-NUS-DIRP/9010100347), the Singapore-MIT Alliance of Research and Technology (SMART) program, and the Economic Development Board (SPORE, COY-15-EWI-RCFSA/N197-1) under National Research Foundation Singapore.

REFERENCES

(1) Cobley, C. M.; Chen, J.; Cho, E. C.; Wang, L. V.; Xia, Y. N. *Chem. Soc. Rev.* **2011**, *40*, 44−56.
(2) Ehrenreich, H.; Philipp, H. *Phys. Rev.* **1962**, *128*, 1622−1629.
(3) Link, S.; El-Sayed, M. A. *J. Phys. Chem. B* **1999**, *103*, 8410−8426.
(4) Kelly, K. L.; Coronado, E.; Zhao, L. L.; Schatz, G. C. *J. Phys. Chem. B* **2003**, *107*, 668−677.
(5) Halas, N. J.; Lai, S.; Chang, W. S.; Link, S.; Nordlander, P. *Chem. Rev.* **2011**, *111*, 3913−3961.
(6) Ghosh, S. K.; Pal, T. *Chem. Rev.* **2007**, *107*, 4797−4862.
(7) Zhao, J.; Pinchuk, A. O.; Mcmahon, J. M.; Li, S. Z.; Ausman, L. K.; Atkinson, A. L.; Schatz, G. C. *Acc. Chem. Res.* **2008**, *41*, 1710−1720.
(8) Noguez, C. *J. Phys. Chem. C* **2007**, *111*, 3806−3819.
(9) Kumar, G. V. P. *J. Nanophoton.* **2012**, *6*, 064503−20.
(10) Camden, J. P.; Dieringer, J. A.; Zhao, J.; Vanduyne, R. P. *Acc. Chem. Res.* **2008**, *41*, 1653−1661.
(11) Polavarapu, L.; Xu, Q.-H. *Langmuir* **2008**, *24*, 10608−10611.
(12) Cheng, D. M.; Xu, Q.-H. *Chem. Commun.* **2007**, 248−250.
(13) Yuan, P. Y.; Lee, Y. H.; Gnanasammandhan, M. K.; Guan, Z. P.; Zhang, Y.; Xu, Q.-H. *Nanoscale* **2012**, *4*, 5132−5137.
(14) Ming, T.; Chen, H.; Jiang, R.; Li, Q.; Wang, J. F. *J. Phys. Chem. Lett.* **2012**, *3*, 191−202.
(15) Su, H.; Zhong, Y.; Ming, T.; Wang, J.; Wong, K. S. *J. Phys. Chem. C* **2012**, *116*, 9259−9264.
(16) Zhang, J.; Lakowicz, J. R. *Opt. Express* **2007**, *15*, 2598−2606.
(17) Mooradian, A. *Phys. Rev. Lett.* **1969**, *22*, 185−187.
(18) Boyd, G.; Yu, Z.; Shen, Y. *Phys. Rev. B* **1986**, *33*, 7923−7936.
(19) Wang, H. F.; Hufft, T. B. H.; Zweifelt, D. A. Z.; Het, W. H.; Lowt, P. S. L.; Weit, A. W.; Xin, C. J. *Proc. Natl. Acad. Sci. U.S.A.* **2005**, *102*, 15752−15756.
(20) Kuo, W. S.; Chang, C. N.; Chang, Y. T.; Yang, M. H.; Chien, Y. H.; Chen, S. J.; Yeh, C. S. *Angew. Chem., Int. Ed.* **2010**, *49*, 2711−2715.
(21) Jang, B.; Park, J.; Tung, C. H.; Kim, I.; Choi, Y. D. *Acs Nano* **2011**, *5*, 1086−1094.
(22) Huang, X.; El-Sayed, I. H.; Qian, W.; El-Sayed, M. A. *J. Am. Chem. Soc.* **2006**, *128*, 2115−2120.
(23) Choi, W. I.; Sahu, A.; Kim, Y. H.; Tae, G. *Ann. Biomed. Eng.* **2011**, *40*, 534−546.
(24) Durr, N. J.; Larson, T.; Smith, D. K.; Korgel, B. A.; Sokolov, K.; Yakar, A. B. *Nano Lett.* **2007**, *7*, 941−945.
(25) Zhao, T. T.; Shen, X. Q.; Li, L.; Guan, Z. P.; Gao, N. Y.; Yuan, P. Y.; Yao, S. Q.; Xu, Q.-H.; Xu, G. Q. *Nanoscale* **2012**, *4*, 7712−9.
(26) Vankayala, R.; Sagadevan, A.; Vijayaraghavan, P.; Kuo, C. L.; Hwang, K. C. *Angew. Chem., Int. Ed.* **2011**, *50*, 10640−10644.
(27) Zhang, H.; Wang, D. *Angew. Chem., Int. Ed.* **2008**, *47*, 3984−3987.
(28) Zhang, Z.; Wu, Y. *Langmuir* **2010**, *26*, 9214−9223.
(29) Pramod, P.; Thomas, K. G. *Adv. Mater.* **2008**, *20*, 4300−4305.
(30) Lin, S.; Li, M.; Dujardin, E.; Girard, C.; Mann, S. *Adv. Mater.* **2005**, *17*, 2553−2559.
(31) Kong, R.-M.; Zhang, X.-B.; Chen, Z.; Tan, W. *Small* **2011**, *7*, 2428−2436.
(32) Yang, M.; Chen, G.; Zhao, Y.; Silber, G.; Wang, Y.; Xing, S.; Han, Y.; Chen, H. *Phys. Chem. Chem. Phys.* **2010**, *12*, 11850−11860.
(33) Cho, E. C.; Choi, S.-W.; Camargo, P. H. C.; Xia, Y. N. *Langmuir* **2010**, *26*, 10005−10012.

(34) Thomas, K. G.; Barazzouk, S.; Ipe, B. I.; Joseph, S. T. S.; Kamat, P. V. *J. Phys. Chem. B* **2004**, *108*, 13066−13068.
(35) Kou, X.; Zhang, S.; Yang, Z.; Tsung, C.-K.; Stucky, G. D.; Sun, L.; Wang, J.; Yan, C. *J. Am. Chem. Soc.* **2007**, *129*, 6402−6404.
(36) Prasad, B. L. V.; Stoeva, S. I.; Sorensen, C. M.; Klabunde, K. J. *Langmuir* **2002**, *18*, 7515−7520.
(37) Darbha, G. K.; Singh, A. K.; Rai, U. S.; Yu, E.; Yu, H.; Ray, P. C. *J. Am. Chem. Soc.* **2008**, *130*, 8038−8043.
(38) Xia, F.; Zuo, X.; Yang, R.; Xiao, Y.; Kang, D.; Vallée-Bélisle, A.; Gong, X.; Yuen, J. D.; Hsu, B. B. Y.; Heeger, A. J.; Plaxco, K. W. *Proc. Natl. Acad. Sci. USA* **2010**, *107*, 10837−10841.
(39) Li, C. M.; Li, Y. F.; Wang, J.; Huang, C. Z. *Talanta* **2010**, *81*, 1339−1345.
(40) Abbas, A.; Tian, L. M.; Kattumenu, R.; Halim, A.; Singamaneni, S. *Chem. Commun.* **2012**, *48*, 1677−1679.
(41) Luo, Y. L.; Shiao, Y. S.; Huang, Y. F. *Acs Nano* **2011**, *5*, 7796−7804.
(42) Fang, W.; Yang, J.; Gong, J.; Zheng, N. *Adv. Funct. Mater.* **2012**, *22*, 842−848.
(43) Yang, X.; Liu, X.; Liu, Z.; Pu, F.; Ren, J.; Qu, X. *Adv. Mater.* **2012**, *24*, 2890−2895.
(44) Guan, Z.; Gao, N.; Jiang, X.-F.; Yuan, P.; Han, F.; Xu, Q.-H. *J. Am. Chem. Soc.* **2013**, *135*, 7272−7277.
(45) Han, F.; Guan, Z. P.; Tan, T. S.; Xu, Q.-H. *ACS Appl. Mater. Interfaces* **2012**, *4*, 4746−4751.
(46) Guan, Z. P.; Li, S.; Cheng, P. B. S.; Zhou, N.; Gao, N. Y.; Xu, Q.-H. *ACS Appl. Mater. Interfaces* **2012**, *4*, 5711−5716.
(47) Guan, Z. P.; Polavarapu, L.; Xu, Q.-H. *Langmuir* **2010**, *26*, 18020−18023.
(48) Jiang, Y. Q.; Horimoto, N. N.; Imura, K.; Okamoto, H.; Matsui, K.; Shigemoto, R. *Adv. Mater.* **2009**, *21*, 2309−2313.
(49) Jiang, X.-F.; Pan, Y.; Jiang, C.; Zhao, T.; Yuan, P.; Venkatesan, T.; Xu, Q.-H. *J. Phys. Chem. Lett.* **2013**, *4*, 1634−1638.
(50) Jiang, C. F.; Guan, Z. P.; Lim, S. Y.; Polavarapu, L.; Xu, Q.-H. *Nanoscale* **2011**, *3*, 3316−3320.
(51) Frens, G. *Nat. Phys. Sci.* **1972**, *241*, 20−22.
(52) Zhang, F. X.; Han, L.; Israel, L. B.; Daras, J. G.; Maye, M. M.; Ly, N. K.; Zhong, C.-J. *Analyst* **2002**, *127*, 462−465.
(53) Jana, N., R.; Gearheart, L.; Murphy, C. J. *J. Phys. Chem. B* **2001**, *105*, 4065−4067.
(54) Nikoobakht, B.; El-Sayed, M. A. *Chem. Mater.* **2003**, *15*, 1957−1962.
(55) Gou, L. F.; Murphy, C. J. *Chem. Mater.* **2005**, *17*, 3668−3672.
(56) Sun, Z. H.; Ni, W. h.; Yang, Z.; Kou, X. S.; Li, L.; Wang, J. F. *Small* **2008**, *4*, 1287−1292.
(57) Huang, X. H.; Neretina, S.; El-Sayed, M. A. *Adv. Mater.* **2009**, *21*, 4880−4910.
(58) Zhang, S. Z.; Kou, X. S.; Yang, Z.; Shi, Q. H.; Stucky, G. D.; Sun, L. D.; Wang, J. F.; Yan, C. H. *Chem. Commun.* **2007**, 1816−1818.
(59) Marinica, D. C.; Kazansky, A. K.; Nordlander, P.; Aizpurua, J.; Borisov, A. G. *Nano Lett.* **2012**, *12*, 1333−1339.
(60) Xing, C. F.; Xu, Q. L.; Tang, H. W.; Liu, L. B.; Wang, S. *J. Am. Chem. Soc.* **2009**, *131*, 13117−13124.
(61) Zijlstra, P.; Chon, J. W. M.; Gu, M. *Nature* **2009**, *459*, 410−413.
(62) Mohamed, M. B.; Volkov, V.; Link, S.; El-Sayed, M. A. *Chem. Phys. Lett.* **2000**, *317*, 517−523.
(63) Jain, P. K.; El-Sayed, I. H.; El-Sayed, M. A. *Nano Today* **2007**, *2*, 18−29.